Application of DSMC Electronic Excitation Modeling to Tangent Slab Radiation Calculation of Hypersonic Reentry Flows

Zheng Li, Ilyoup Sohn, Deborah A. Levin* and Michael F. Modest†

*Department of Aerospace Engineering, The Pennsylvania State University, University Park, PA 16802
†School of Engineering, University of California, Merced, CA 95343

Abstract. The current work implemented excited levels of atomic N and corresponding electron impact excitation/de-excitation and ionization processes in DSMC. Results show that when excitation models are included, the Starduct 68.9 km re-entry flow has an observable change in the ion number densities and electron temperature. Adding in the excited levels of atoms improves the degree of ionization by providing additional intermediate steps to ionization. The extra ionization reactions consume the electron energy and reduce the electron temperature. The DSMC results of number densities of excited levels are lower than the prediction of quasi steady state calculation. Comparison of radiation calculations using electronic excited populations from DSMC and QSS indicates that, at the stangation point, there is about 20 % difference of the radiative heat flux between DSMC and QSS.

Keywords: DSMC, Kinetic Theory, Radiation
PACS: 47.55.Ca

INTRODUCTION

For high-speed reentry vehicles, such as Stardust[1], ionization and radiation effects are important for the high-efficiency design of heat shield. Due to the fact that high Mach number hypersonic reentry flows are from transitional to continuum, radiation plays an important role in generating heat, in addition to heat transfer.

In the past, the Stardust mission, entering the atmosphere at 12.8 km/s, has been the task of postflight analysis to estimate the validity of flow solver using finite volume scheme and the Nonequilibrium air radiation (NEQAIR) code [2], which is a line-by-line based radiation solver in an uncoupled manner [3]. Recently, coupled radiation calculation with chemically reacting flow model, using the Data Parallel Line Relaxation (DPLR)[4] code and newly developed line-by-line database based on NEQAIR [5], for the Stardust peak heating conditions was performed [6].

Under the transient flow and strong shock condition, continuum breakdown occurs. Therefore, alternative to CFD technique, particle methods, such as direct simulation Monte Carlo (DSMC)[7] method, are required to accurately simulate high-speed reentry flow at high altitude. In our recent work, DSMC simulations with charged species was coupled with the particle based photon Monte Carlo (p-PMC) method, [8] using the efficient spectral modules[9] or with the FV-PMC methods[10] for the Stardust reentry flow conditions.

Although the radiation calculation was improved using the PMC methods in the above calculations, one assumed particles to be in electronically ground level in DSMC and the electronically excited populations were obtained by using either the Boltzmann distribution or the quasi steady state (QSS) method[11]. For the modeling of the radiation and chemical reactions, electronic excitation processes need to be correctly modeled in order to accurately predict the flow field. Most DSMC calculations assumed particles to be in the electronically ground state, and energies are assigned to only translational, rotational, and vibrational modes. However, since the hypersonic flows are energetic, the addition of electronic modes can change the flow field as well as predict radiation and chemical reaction effects. Because the ionization rates from electronically excited levels are generally higher that those from the ground level,[12] the addition of electronically excited levels and electronic transitions to DSMC will change the flow field prediction.

From our previous research,[8, 10] atomic excitation and radiation are known to be more important for the energetic earth reentry flows compared to molecular radiation. Therefore, in this work, atomic excited levels and electronic excitation processes are modeled in DSMC and different chemical reaction rates are modeled for each electronic level. For each electronic transition, excitation and de-excitation cross sections are investigated, and the electronic excitation populations are controlled by the cross sections.

IMPLEMENTATION OF ATOMIC EXCITATION IN DSMC

The very first step to implement atomic excitation in DSMC is to identify the important electronic levels for the atomic species which, in this work, are atomic nitrogen, N, and atomic oxygen, O. In NEQAIR [2], 22 electronic levels are considered for N and 19 for O. However, from our previous investigation on the N and O spectral radiation[9, 10], for N two electronic excited levels, 4th (120 nm) and 5th (113.4 nm), and, for O, 5th (130.4 nm) and 9th (102.7 nm), were found to be important. Therefore, for N, the corresponding electronic levels, 1st (ground), 4th (excited), 5th (excited) and continuum (ionized) levels, and electronic transition processes are implemented in the DSMC and are shown in Fig. 1. Likewise, corresponding levels and transitions are implemented for O. In the DSMC implementation, an index of electronic level, i, is assigned for each DSMC atomic particle.

In Fig. 1, atomic N gets excited and de-excited by collisional (K(i,j)) and radiative (A(i,j)) processes. When an atom collides with another atom, a molecule, or an electron, its electronic levels can potentially change. Collision-induced electronic transitions in an atomic or molecular system are particularly effective when the collider is an electron. Particularly, when a free electron with high energy collides with an atom in a bound state, the energy of the free electron can be transferred to the atom through the process of electronic excitation. In this case, the excitation rate from the initial state i to the final state j is $K(i,j)N_iN_e$. A summary of the excitation/de-excitation and ionization processes of atomic N, studied in this work, may be written as,

$$\mathrm{N}(1)+e^- \xrightarrow{K(1,4)} \mathrm{N}(4)+e^- \tag{1}$$

$$\mathrm{N}(1)+e^- \xrightarrow{K(1,5)} \mathrm{N}(5)+e^- \tag{2}$$

$$\mathrm{N}(4)+e^- \xrightarrow{K(4,1)} \mathrm{N}(1)+e^- \tag{3}$$

$$\mathrm{N}(5)+e^- \xrightarrow{K(5,1)} \mathrm{N}(1)+e^- \tag{4}$$

$$\mathrm{N}(1)+e^- \xrightarrow{K(1,c)} \mathrm{N}^+ + 2e^- \tag{5}$$

$$\mathrm{N}(4)+e^- \xrightarrow{K(4,c)} \mathrm{N}^+ + 2e^- \tag{6}$$

$$\mathrm{N}(5)+e^- \xrightarrow{K(5,c)} \mathrm{N}^+ + 2e^- \tag{7}$$

where N(i) and N^+ represent an atomic species of electronic energy level i and its ion, respectively. Similar excitation/de-excitation and ionization processes of atomic O are studied.

After a pair of N(1) and e^- is selected for collision, three processes are possible: excitation, (processes (1) and (2)), ionization (processes (5)) and thermal collision. The excitation takes place under the condition $E_c > E(i)$ with the probability $P_{ex}(i)$. Here E_c is the collision energy or $m_R g^2/2$, m_R is the reduced mass of the N(1) and e^- pair and g is the collision relative velocity. The collision energy can also be written as $m_e v_e^2/2$ as the electron mass is much smaller than the atom mass and electron velocity is much higher than that of an atom. $E(i)$ is the electronic energy difference between levels i and 1 (ground level) and $i > 1$. The individual excitation probability,

$$P_{ex}(i) = \frac{\sigma_{ex}(i)}{\sigma_{VHS}}. \tag{8}$$

The total excitation cross section, σ_{ex}, is calculated as the sum of the individual cross sections, $\sum_i \sigma_{ex}(i)$. σ_{ex} may not be negligible compared to the total, which is represented by the variable hard sphere (VHS) model. the excitation cross sections for the N and O taken from the work of Stone and Zipf[13, 12]. For electron energy under 20 ev, which is the maximum electron energy in the flow considered in this work, the VHS cross sections of N is in the range of 21 - 5 Å^2, therefore, the excitation probability is from 0 to 25%. Similarly, the upper limit of the excitation probability for O is 26%. Once the pair is determined to undergo the excitation process, the collision energy E_c is reduced by the electronic energy difference $E(i)$ to $E_c' = E_c - E(i)$. The velocities of the atom N(i) and electron e^-, $\vec{v}'_{\mathrm{N(i)}}$ and $\vec{v}'_e$, are determined from the momentum and energy conservation laws

$$m_{\mathrm{N}}\vec{v}'_{\mathrm{N(i)}} + m_e\vec{v}'_e = m_{\mathrm{N}}\vec{v}_{\mathrm{N(1)}} + m_e\vec{v}_e \tag{9}$$

$$\vec{v}'_{\mathrm{N(i)}} - \vec{v}'_e = \left(\frac{2E_c'}{m_R}\right)^{1/2}\vec{e} \tag{10}$$

where $\vec{e}$ is a random unit vector. Thus, the post-excitation collision energy is transformed into the energy of the relative motion of the atom N(i) and electron e^-.

The ionization (process (5)) occurs when the collision energy E_c is greater than the ionization energy E_∞ with the probability

$$P_{ion} = \frac{\sigma_{ion}}{\sigma_{VHS}}. \tag{11}$$

Figures 2 show the ionization cross sections for the N taken from the work of Kim[14]. For low electron energy, the ionization cross sections are significantly lower than those of excitation as the ionization threshold E_∞ is higher than excitation threshold $E(i)$. When the pair of N(1) and electron e^- is determined to have a ionization reaction, firstly, the collision energy E_c is reduced to to $E_c' = E_c - E_\infty$. Then an inelastic collisions between N(1) and e^- is performed based on momentum and energy conservation laws and the post-collisional velocities of N(1) and e^- are $\vec{v}^*_{\mathrm{N(i)}}$ and $\vec{v}^*_e$. The last stage of the ionization process is that the N(1) atom decomposes into an N^+ ion and another e^-. The velocities of the ion N^+ and electron e^- are determined as

$$\vec{v}'_{\mathrm{N}^+} = \vec{v}'_e = \vec{v}^*_{\mathrm{N(1)}}. \tag{12}$$

The thermal collision cross section, σ_{el}, for a collision pair of N(1) and electron e^- is then calculated as

$$\sigma_{el} = \sigma_{VHS} - \sigma_{ex} - \sigma_{ion} \tag{13}$$

When the pair is not determined to undergo excitation or ionization process, the pair will simply have the thermal collision or elastic collision as both colliders have no internal energies. This process occurs most of the time as the excitation and ionization cross sections are relatively small compared to the total (VHS) cross section. The post-collisional velocities are determined as

$$m_{\mathrm{N}}\vec{v}'_{\mathrm{N(1)}} + m_e\vec{v}'_e = m_{\mathrm{N}}\vec{v}_{\mathrm{N(1)}} + m_e\vec{v}_e \tag{14}$$

$$\vec{v}'_{\mathrm{N(1)}} - \vec{v}'_e = \left(\frac{2E_c}{m_R}\right)^{1/2}\vec{e}. \tag{15}$$

In addition, when an excited-level atom, N(i), collides with another particle, the collision is treated in the same way as a ground-level atom, N(1), collides with another particle and the electric level will remain the same. However, when an excited-level atom reacts with another particle, if it is an exchange reaction, such as NO + N(i) $\rightarrow$ N_2 + O, the electronic energy is added to the collision energy to determine the reaction probability and, if a reaction occurs, is treated as internal energy and will be released as an addition to the reaction heat. If the reaction is an dissociation reaction, such as N(i) + O_2 $\rightarrow$ N(i) + O + O, the electric level will remain the same and no electronic energy shall be released.

FLOW FIELD RESULTS AND DISCUSSION

In the flow modeling, 15 species (N, O, C, N^+, O^+, N_2, O_2, NO, CO, CN, CO_2, N_2^+, O_2^+, NO^+, and e^-) are considered for the Stardust blunt body re-entry flow. Figure 3 shows the Stardust blunt body geometry that is studied in this work and the flow condition is listed in Table 1. The DSMC method is implemented in the Statistical Modeling In Low-density Environment (SMILE)[15] computational tool. Two DSMC simulations of the Stardust re-entry flow at 68.9 km altitude are then performed with and without the atomic excitation. Note here that the radiative processes are not modeled in this comparison.

Figure 4 shows distribution of the translational, rotational, vibrational and electron temperatures along the stagnation line with and without atomic excitation. It can be seen from the upper left part, the translational temperature is the highest and the rotational, vibrational and electron temperatures are close. There is no difference of the translational temperatures between the simulations with and without atomic excitation (see upper right part). When comparing the rotational and vibrational temperatures (lower left), the rotational temperature with atomic excitation is slightly higher than that without excitation and the vibrational temperature is on the opposite side. The electron temperature with excitation, however, can be seen to have more than 10% difference from the one without excitation which is due to the fact the excitation reactions consume electron energy.

Figure 5 show the total, ion and electron number densities with and without excitation. The ion and electron number densities, in general, are close to each other for both cases, as the average ion velocity model is applied to the movement of the electrons. Since the density of the major species in the near body, atomic N, is the same for both simulations, the total number density has no change when excitation is added. The ion number density changes significantly as the N^+ increases significantly with a maximum of 40% when atomic excitation is applied. Adding in the excited levels of atoms improves the ion number densities or the degree of ionization by providing additional intermediate steps to ionization. The extra ionization reactions consume the electron energy and reduce the electron temperature.

The ion, electron, atom number densities and the electron temperature in each cell along the stagnation line from the non-excitation DSMC calculation are put into QSS calculations. The rates in the NEQAIR are modified so that they match the cross sections used in the DSMC calculations. Radiative decay is firstly ignored in QSS as they are not modeled in DSMC. Figure 6 shows comparisons of number densities of N(4) and N(5) from DSMC and QSS calculations with and without radiative decay. In the left part of the figure, the QSS results are smooth as the input variables are smooth and it is a non-statistical method while DSMC results have a quite large statistical error. The QSS predicts higher N(4) number density than that N(5) and both are different from those from DSMC. The DSMC predicts a slight higher N(5) density than N(4). Also DSMC predicts a higher N(4) and N(5) number densities than QSS before $X = -0.015m$ but lower number densities after $X = -0.015m$. The difference between DSMC and QSS results may also due to the fact that DSMC uses cross sections and the does not assume that electron velocity has a Maxwellian distribution.

RADIATION CALCULATIONS USING ELECTRONIC EXCITED POPULATIONS IMPLEMENTED ON DSMC

In this section, radiation is calculated using the electronic state populations implemented on DSMC excitation modeling. The analysis of radiative heating to the Stardust blunt body has been performed using established radiation models such as the Langley Optimized Radiative Nonequilibrium (LORAN) code[16] and the Nonequilibrium Air Radiation (NEQAIR) code[2]. These radiation models can generate the electronic excite populations of atomic and molecular species using the Boltzmann or non-Boltzmann relationship, which use an internal temperature and species concentrations on the ground level from the flowfield solution. In this work, the electronic state populations calculated from DSMC are directly used to calculate radition. The tangent slab (TS) approximation is employed to solve the radiative transport equation (RTE), using the exact analytical solutions based on exponential integrals[17]. The Einstein transitional probability data for bound-bound transitions are taken from NEQAIR and only bound-bound radiation is considered because the continuum radiation is much less contributed to total radiation than atomic line radiation. The Voigt line shape is used to describe the thermal and electron collsion induced line broadening. Since DSMC only implemented two excited states for atomic N and O as previously discussed, six bound-bound transition data related to the two excited states are extracted from NEQAIR for each atomic N and O species.

Figure 7 shows the total emission and radiative heat flux of the mixed atomic N and O species along the stagnation line of the Stardust blunt body using DSMC and QSS population data. The total emission using QSS populations is observed to be higher than the emission using the excited populations implemented on DSMC from x=-0.45 to -1.55 cm due to higher electronic state populations from QSS. Atomic O emission contributes to the total emission approximately by 3 % for both DSMC and QSS cases. Two distributions of radiative heat flux along the stagnation line from DSMC and QSS have similar pattern except the region from x=-0.25 to -0.85 cm. At the stangation point, there is about 20 % difference of the radiative heat flux between DSMC and QSS. The radiative heat flux calculated using the chosen two levels of electronic state population is approximately 50 % of the radiative heat flux considering all electronic excited levels and transitions.

SUMMARY

The current work implemented excited levels of atomic N and corresponding electron impact excitation/de-excitation and ionization processes in DSMC. Results show that when excitation models are included, the Starduct 68.9 km re-entry flow has an observable change in the ion number densities and electron temperature. Adding in the excited levels of atoms improves the degree of ionization by providing additional intermediate steps to ionization. The extra ionization reactions consume the electron energy and reduce the electron temperature. The DSMC results of number densities of excited levels are different from those predicted by of QSS and it is due to the non-equilibrium characteristics of the flow. Comparison of radiation calculations using electronic excited populations from DSMC and

QSS indicates that, at the stangation point, there is about 20 % difference of the radiative heat flux between DSMC and QSS.

ACKNOWLEDGMENTS

The research performed at the Pennsylvania State University was supported by the NASA through the Grant No. NNX07AC47A. We would like to acknowledge Prof. M. Ivanov of the Institute of Theoretical and Applied Mechanics, Russia for the use of the original SMILE code.

REFERENCES

1. D. Olynick, Y. Chen, and M. Tauber, *Journal of Spacecraft and Rockets* **36**, 442–462 (1999), ISSN 0022-4650.
2. C. Park, and A. R. Center., *Nonequilibrium Air Radiation (NEQAIR) Program [microform] : user's manual / Chul Park*, National Aeronautics and Space Administration, Ames Research Center ; For sale by the National Technical Information Service, Moffett Field, Calif. : [Springfield, Va. :, 1985.
3. Y. Liu, D. Prabhu, K. Trumble, and D. Saunders, Radiation modeling for the reentry of the stardust sample return capsule, AIAA paper 2008-1213 (2008).
4. *AIAA Journal* **36**, 1603–1609 (1998), ISSN 0001-1452.
5. I. Sohn, A. Bansal, M. Modest, and D. Levin, Advanced radiation calculations of hypersonic reentry flows using efficient databasing schemes, AIAA paper 2008-4019 (2008).
6. A. Feldick, M. Modest, and D. Levin, Closely coupled flow field-radiation interactions for flowfields created during hypersonic reentry, AIAA paper 2008-4104 (2008).
7. G. A. Bird, *Molecular Gas Dynamics and the Direct Simulation of Gas Flows*, Clarendon Press, 1994.
8. T. Ozawa, A. Wang, D. A. Levin, and M. F. Modest, Development of a coupled dsmc-particle photon monte carlo method for simulating atomic radiation in hypersonic reentry flows, AIAA paper 2008-3916 (2008).
9. T. Ozawa, D. A. Levin, and M. F. Modest (2008).
10. I. Sohn, T. Ozawa, D. A. Levin, and M. F. Modest, Dsmc hypersonic reentry flow simulations with photon monte carlo radiation, AIAA paper 2009-1566 (2009).
11. C. Park, *Nonequilibrium Hypersonic Aerothermodynamics*, Wiley-Interscience, 1990.
12. W. M. Huo, Electron recombination and collisional excitation in air, AIAA paper 2009-1593 (2009).
13. E. J. Stone, and E. C. Zipf, *The Journal of Chemical Physics* **58**, 4278–4284 (1973), URL `http://link.aip.org/link/?JCP/58/4278/1`.
14. Y.-K. Kim, *Physical Review A* **66** (2002), 012708.
15. M. S. Ivanov, A. V. Kashkovsky, S. F. Gimelshein, G. N. Markelov, A. A. Alexeenko, Y. A. Bondar, G. A. Zhukova, S. B. Nikiforov, and P. V. Vashenkov, "SMILE System for 2D/3D DSMC computations," in *Proceedings of the 25th International Symposium on Rarefied Gas Dynamics*, edited by M. S. Ivanov, and A. K. Rebrov, Publishing House of the Siberian Branch of the Russian Academy of Sciences, Novosibirsk, 2007, pp. 539–544.
16. L. C. Hartung, *Journal of Thermophysics and Heat Transfer* **6**, 618–625 (1992), ISSN 0887-8722.
17. M. F. Modest, *Radiative Heat Transfer (2nd edition)*, Academic Press, New York, 2003.

TABLE 1. Free Stream parameters

Parameter	68.9 km
Temperature, K	224
Number density, molec/m^3	1.6028×10^{21}
Speed, km/s	11.9
O_2 mole fraction, %	23.72
N_2 mole fraction, %	76.28
$K_{n,\infty}(L = 0.22$ m)	0.017

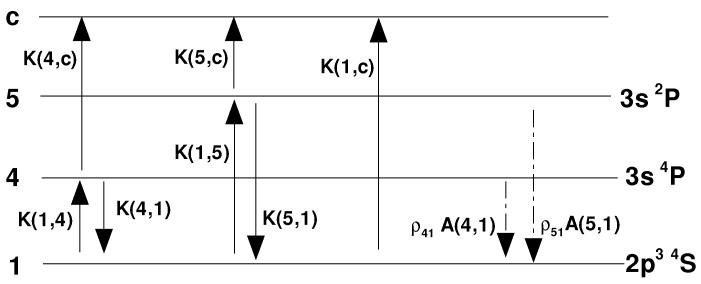

FIGURE 1. Collisional and radiative transitions of atomic N modeled in this work.

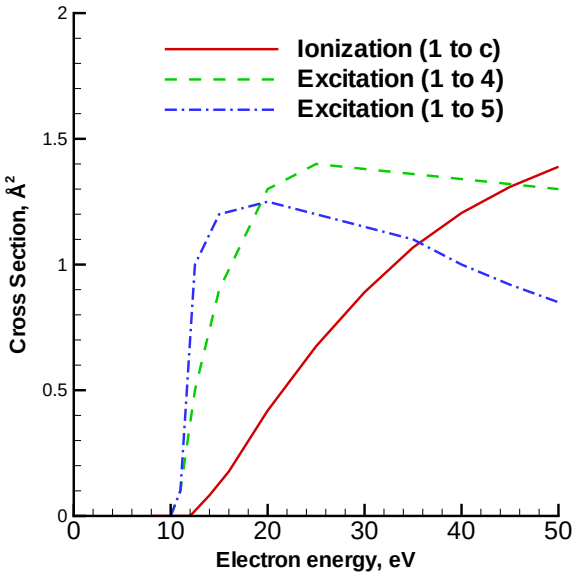

FIGURE 2. Comparison of ionization and two electronic excitation (1 to 4 and 1 to 5) cross sections for N as a function of electron energy.

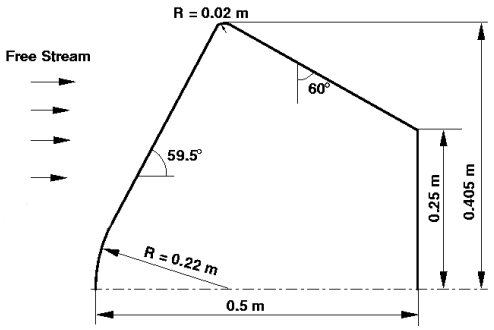

FIGURE 3. Stardust Geometric Configuration.

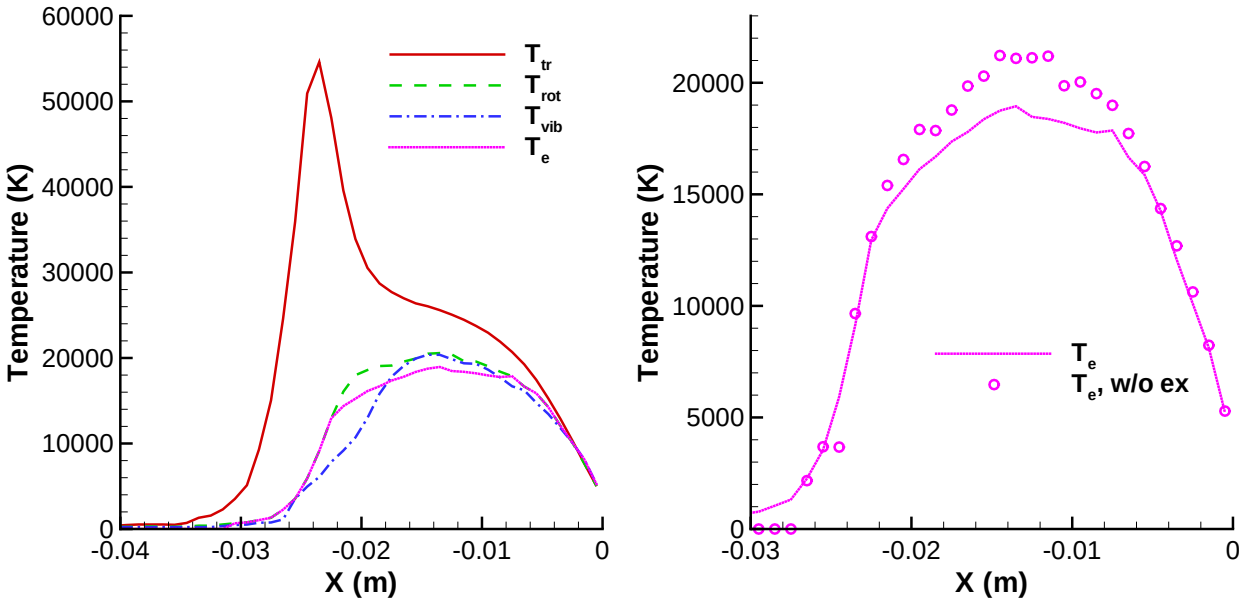

FIGURE 4. Distribution of the translational, rotational, vibrational and electron temperatures along the stagnation line for the Stardust blunt body at 68.9 km altitude with and without atomic excitation.

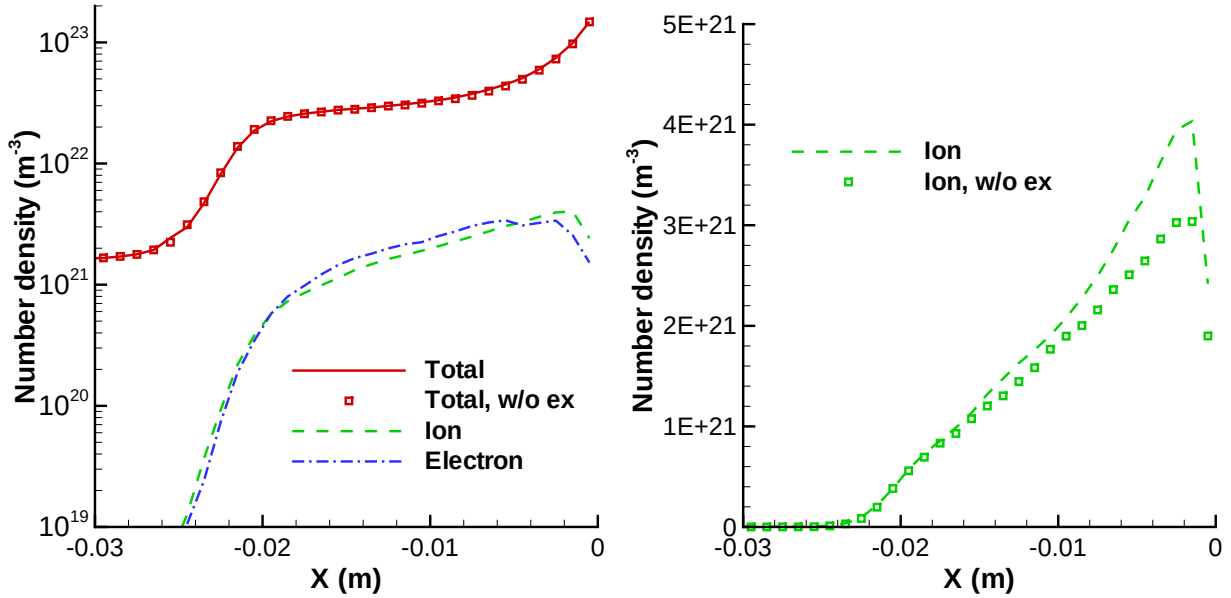

FIGURE 5. Distribution of total, ion, and electron number densities along the stagnation line for the Stardust blunt body at 68.9 km altitude with and without atomic excitation.

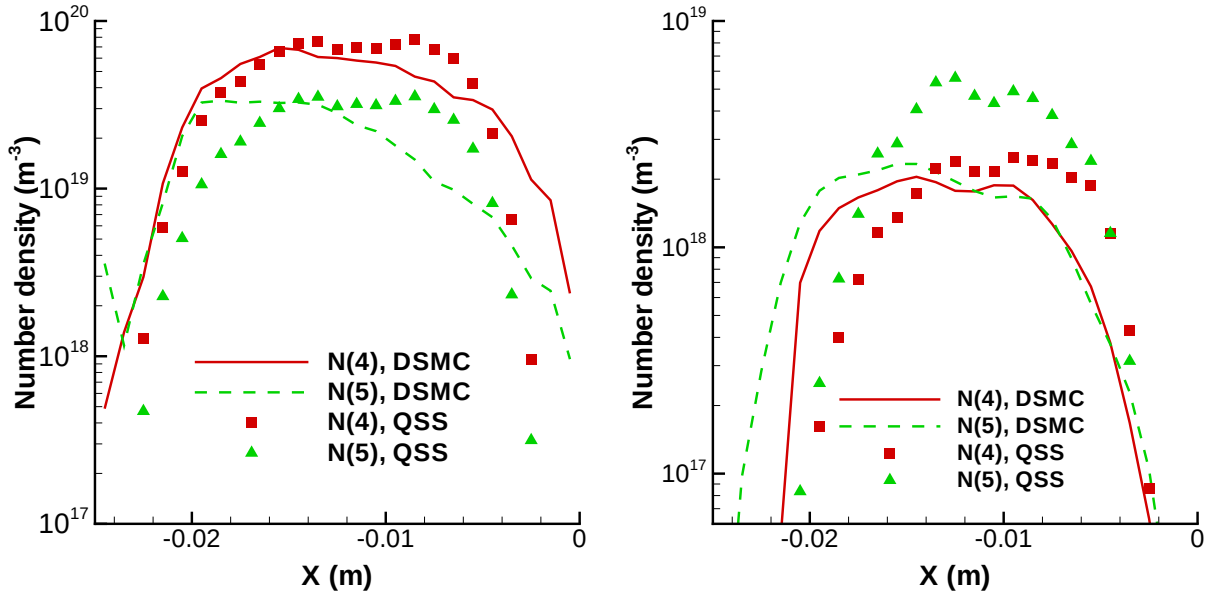

FIGURE 6. Distribution of N (4) and N (5) number densities along the stagnation line for the Stardust blunt body at 68.9 km altitude from DSMC and QSS calculations without (left) and with radiative decay (right).

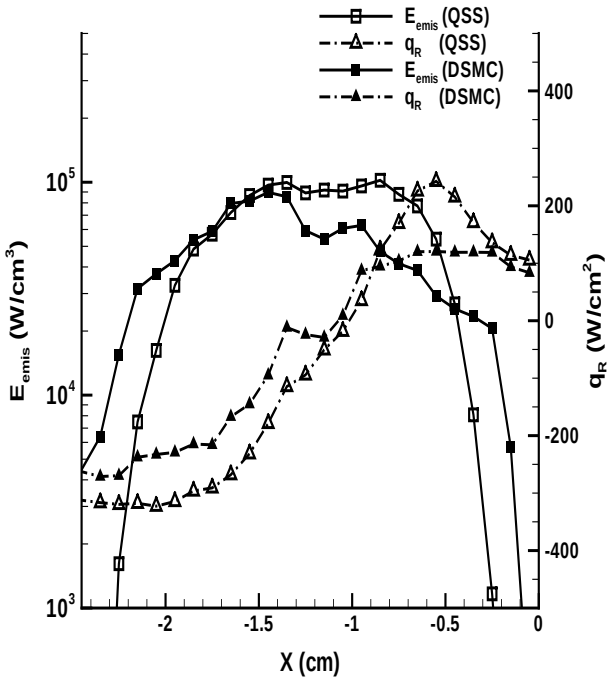

FIGURE 7. Comparison of total emission and radiative heat flux of the mixed atomic N and O species along the stagnation line of the Stardust blunt body using DSMC and QSS populations.